Analysis of ARAIM Against EOP GPS-Galileo Faults on LPV-200 Precision Approach

Santiago Perea Díaz[†], Mathieu Joerger[*], Boris Pervan[*], Markus Rippl[†] and Ilaria Martini[†]
[†]*Institute of Communications and Navigation, German Aerospace Center (DLR)*
[*]*Illinois Institute of Technology*

BIOGRAPHY

Santiago Perea Díaz obtained a Master of Science in Aerospace Engineering from University of Sevilla (Spain) in 2013. In parallel, as a double degree student, he gained his Master in Mechanical and Aerospace Engineering from Illinois Institute of Technology (IIT) in 2013. Currently he is part of the staff at the Institute of Communications and Navigation at German Aerospace Center (DLR). His research focuses on new advanced algorithms for multi-constellation Residual Autonomous Integrity Monitoring (RAIM).

Dr. Mathieu Joerger obtained a Master in Mechatronics from the National Institute of Applied Sciences in Strasbourg, France, in 2002, and a M.S. and a Ph.D. in Mechanical and Aerospace Engineering from the Illinois Institute of Technology (IIT), in 2002 and 2009 respectively. He is the 2009 recipient of the Institute of Navigation (ION) Bradford Parkinson award, which honors outstanding graduate students in the field of GNSS. He is currently a research assistant professor at IIT, working on multi-sensor integration, on sequential fault-detection for multi-constellation navigation systems, and on relative and differential receiver autonomous integrity monitoring (RAIM) for shipboard landing of military aircraft.

Dr. Boris Pervan is a Professor of Mechanical and Aerospace Engineering at IIT, where he conducts research on advanced navigation systems. Prior to joining the faculty at IIT, he was a spacecraft mission analyst at Hughes Aircraft Company (now Boeing) and a postdoctoral research associate at Stanford University. Prof. Pervan received his B.S. from the University of Notre Dame, M.S. from the California Institute of Technology, and Ph.D. from Stanford University. He is an Associate Fellow of the AIAA, a Fellow of the Institute of Navigation (ION), and Editor-in-Chief of the ION journal NAVIGATION. He was the recipient of the IIT Sigma Xi Excellence in University Research Award (2011, 2002), Ralph Barnett Mechanical and Aerospace Dept. Outstanding Teaching Award (2009, 2002), Mechanical and Aerospace Dept. Excellence in Research Award (2007), University Excellence in Teaching Award (2005), IEEE Aerospace and Electronic Systems Society M. Barry Carlton Award (1999), RTCA William E. Jackson Award (1996), Guggenheim Fellowship (Caltech 1987), and Albert J. Zahm Prize in Aeronautics (Notre Dame 1986).

Markus Rippl received his Diploma in Electrical Engineering and Information Technology from Technische Universitat Munchen (TUM) in 2007. Since then, he has been a research associate with the Institute of Communications and Navigation at the German Aerospace Center (DLR), in Oberpfaffenhofen near Munich. His field of work is the integrity of GNSS-based navigation using receiver-side algorithms.

Dr. Ilaria Martini received the Master Degree in telecommunication engineering and the Ph.D. in information technology from the University of Florence, Italy. She was at the Galileo Project Office of ESA/ESTEC in 2003, working on the performance of the Galileo Integrity Processing Facility. She was research associate in 2004 at the University of Florence and in 2005 at the Institute of Geodesy and Navigation of the Federal Armed Forces Germany in Munich. In 2006 she joined the navigation project department of Ifen GmbH in Munich. Since 2012 she works as research associate in the Institute of Communication and Navigation at the German Aerospace Center (DLR), Oberpfaffenhofen. Her main area of interest is GNSS Integrity Monitoring.

ABSTRACT

This paper presents a detection algorithm for constellation faults on LPV-200 precision approach. In particular, this work focuses on the Earth Orientation Parameters (EOP) faults which are the only Constellation Wide Fault listed in the current GPS Standard Positioning Service and Performance Standard. These faults are particularly hazardous for single-constellation RAIM algorithms since they cannot be detected by measurement redundancy. This paper investigates the properties of the rotation of the ephemeris-based satellite positions caused by EOP fault and its impact in the pseudorange fault vector. This work will show that EOP faults are constrained, aspect that can be exploited in

the pseudorange domain. Under a dual constellation GPS-Galileo scenario, we develop an Integrity Risk evaluation method based on Residual Based RAIM specifically designed to account for EOP faults. In addition, this paper investigates different EOP constellation fault scenarios based on the independence of the fault across constellations. We finally show that EOP determination process at the ground and satellite ephemeris updating method play an essential role in the availability performance.

I. INTRODUCTION

The modernization of the GPS constellation with a new generation of satellites along with the development of the emerging Galileo will provide new navigation signals which will enhance the performance of the current navigation systems. The increase in number of signals and frequencies will positively impact the Receiver Autonomous Integrity Monitoring (RAIM) by providing redundant measurements to perform consistency checks. However, the deployment of new constellations and satellites will also entail a reconsideration of the current threat scenario not only concerning satellite but also constellation faults.

Constellation faults are defined as those events when more than one satellite within a core constellation are affected by a common source error [1]. Although they can be seen as an extension of the single satellite fault case, they are of sufficient relevance to be discussed separately. Unlike traditional RAIM algorithms, new generation Advanced RAIM (ARAIM) can perform cross-constellation comparison to account for constellation faults. However, ARAIM algorithms present a particular weakness against constellation faults due to the large size of the faulty measurements subset when analyzing the integrity bound of the corresponding fault hypothesis. It has a significant impact in the availability performance given that either the integrity or accuracy requirement might not be fulfilled.

Previous work has categorized the constellation faults according to their origin: inadequate manned operations, failures inherent to the ground segment and failures induced externally [2]. From all them, only one type has been explicitly identified as a potential integrity failure mode in the current GPS Standard Positioning Service and Performance Standard [3]; Earth Orientation Parameters (EOP) fault. In particular, the ARAIM Technical Subgroup of the EU/US Working Group C (WGC) has already proved that ARAIM could efficiently monitor against EOP faults, assuming that they occur independently across constellations [1]. EOP faults simultaneously affecting both constellations, caused for example by erroneous observational data from an international source, were left unaddressed.

Taking advantage of the particular constraint of this type of constellation faults, this paper analyzes the potential of GPS-Galileo ARAIM to monitor against cross constellation EOP faults. In essence, from the user's perspective, an EOP fault causes a common erroneous apparent rotation of the satellite position. This geometrical property can be exploited in the measurement domain by constraining the pseudorange error vector by a common EOP rotation. The scope of the monitor described in this paper is to quantify the EOP fault contribution to the total Integrity Risk, ultimately enhancing the availability performance.

The first part of the paper formally defines the geometrical transformation of the satellite position caused by an EOP fault. By following a straightforward algebraic derivation, we will show that this specific type of constellation faults constrains the fault vector to lie in a bi-dimensional space in the pseudorange domain. Section III and IV revise the Integrity Risk evaluation for multi-constellation GNSS and the use of the Residual Based RAIM approach against multi-measurements faults. Section V discusses the different EOP constellation fault scenarios reconsidering the independence across constellations. Finally, section VI evaluates the worldwide performance of the EOP fault detector for an example of an aircraft LPV-200 precision approach [4]. Availability maps will highlight the benefits in the fault detection performance when the constellation fault hypothesis is constrained.

II. EOP FAULT CHARACTERIZATION

A. Earth Orientation Parameters

GPS Master Control Stations (MCS) and Galileo Control Center (GCC) need to transform satellite position from International Terrestrial Reference Frame (ITRF) to Geocentric Celestial Reference Frame (GCRF) during satellite orbit determination. For that purpose, orbit determination and time synchronization (ODTS) facilities account for the Earth's rotation axis variability with respect to the inertial space (celestial motion) and with respect to its crust (terrestrial motion) together with the change in the duration of the sidereal days [5]. On one hand, the celestial motion is a consequence of solar and lunar gravitational field variations along the Earth's orbit causing two movements: precession and nutation. These two parameters can accurately be predicted since the orbits and masses of these bodies are known [6]. On the other hand, the terrestrial motion is due to Earth's elastic and geological properties and it needs to be determined empirically.

Earth Orientation Parameters (EOP) are a set of two angles (polar motion x_p and y_p) and a time difference (UT1-UTC) that account for the terrestrial motion of the Earth's rotation axis and the variability of its spin rate respectively. They are computed by the corresponding MCS and GCC using

EOP Predictions (EOPP) provided by an independent service. Although separately computed and monitored, it is still under investigation whether an erroneous EOPP can affect both constellations simultaneously given that they are based on some common measurements. This discussion will be addressed in Section V.

From integrity perspective, the threat of an erroneous conversion from Earth-Centered Inertial (ECI) to Earth-Centerd Earth-Fixed (ECEF) frame resides in the accuracy and reliability of the EOP estimated by the constellation control station. EOP rotation vector will be defined in this study as

$$\boldsymbol{\theta} = \begin{bmatrix} x_p \\ y_p \\ UT1 - UTC \end{bmatrix}. \tag{1}$$

B. EOP fault definition

Analogous to GBAS ephemeris faults, EOP ones are initially classified in Type A and Type B. Both have same general impact on the satellite and user position error but a difference with respect to detection method. This paper only focuses on Type B EOP faults which have their origin in the use of erroneous EOPP in the Orbit Determination. A further description of the fault types is provided in [1].

Under a fault scenario, wrong determination of the EOP values causes an incorrect transformation of the satellites orbital parameters from celestial (ECI) to terrestrial reference frame (ECEF). From the user's point of view, based on ephemeris, the whole constellation undergoes a common rotation representing a challenge for single constellation RAIM monitors. Since those algorithms are based on measurement redundancy, a consistent common rotation makes the fault completely imperceptible through RAIM-type monitors unless an additional constellation is used. In fact, previous work [7] has demonstrated that, for single constellation RAIM, the residual vector generated by pseudorange errors due to a consistent fault is zero (consequently the associated test statistic is also zero). The use of two constellations provides a potential detection method against EOP faults

The observed EOP event on PRN 19 on June 17$^{\text{th}}$, 2012 [8] provides substantial motivation for the need to mitigate this threat. According to the report, the satellite was uploaded with invalid Earth orientation data. If MCS personnel had not detected the anomaly, it would have affected the rest of the constellation by the time they were updated.

C. Geometry of the EOP fault

Now that the physical source of the EOP has been described, let us dive into the geometrical properties of the fault. The aim of this section is to mathematically show that EOP constellation faults are geometrically constrained and hence, the fault vector lies in a specific subspace in the measurement domain.

We first derive the impact of an EOP fault on the pseudorange error in the measurement equation. Once it is done for one satellite, we will extrapolate the derivation to the full constellation. We start with the simple description of the satellite (SV_i) estimated position vector $\hat{\boldsymbol{x}}^i_{SV}$ as the sum of the true satellite position $\boldsymbol{x}^i_{SV}$ and the satellite position error $\delta\hat{\boldsymbol{x}}^i_{SV}$ in ECEF

$$\hat{\boldsymbol{x}}^i_{SV} = \boldsymbol{x}^i_{SV} + \delta\hat{\boldsymbol{x}}^i_{SV}. \tag{2}$$

Let us characterize the second term on the right hand side of (2) as an ephemeris error due to an EOP fault. Earth Orientation Parameters fault manifests itself as an Earth-centered, small angle rotation of the estimate satellite position vector. The first assertion (Earth-centered rotation) is immediate to prove; ECEF-ECI conversion consists in a three dimensional rotation around the center of the Earth. The second statement (small angle rotation) refers to the actual magnitude of the rotation. Historical EOP data provided by the IERS support the assumption of treating EOP faults as an small angle rotation vectors [9].

As a consequence, the ephemeris error can be regarded as an infinitesimal rotation of the satellite true position [10] whose direction and magnitude is defined by the EOP fault rotation vector

$$\delta\hat{\boldsymbol{x}}^i_{SV} = [\delta\boldsymbol{\theta}\times]\hat{\boldsymbol{x}}^i_{SV} \tag{3}$$

where the EOP fault vector and its skew-symmetric form are defined as

$$\delta\boldsymbol{\theta} = \begin{bmatrix} \delta\theta_x \\ \delta\theta_y \\ \delta\theta_z \end{bmatrix} \text{ and} \tag{4}$$

$$[\delta\boldsymbol{\theta}\times] = \begin{bmatrix} 0 & -\delta\theta_z & \delta\theta_y \\ \delta\theta_z & 0 & -\delta\theta_x \\ -\delta\theta_y & \delta\theta_x & 0 \end{bmatrix}. \tag{5}$$

Note that (3) is a cross product of two vectors ($\delta\boldsymbol{\theta} \times \hat{\boldsymbol{x}}^i_{SV}$) expressed in matrix form. The contribution of the EOP fault to the pseudorange error is simply the projection of the satellite position error vector into the Line Of Sight (LOS). An important consequence of the infinitesimal rotation assumption is that the LOS vector between user and corresponding SV_i does not vary in the presence of the EOP rotation. That allows us to write EOP contribution to the pseudorange equation as

$$f^i_{EOP} = (\boldsymbol{e}^i)^T \cdot \delta\hat{\boldsymbol{x}}^i_{SV} = (\boldsymbol{e}^i)^T \cdot [\delta\boldsymbol{\theta}\times]\hat{\boldsymbol{x}}^i_{SV}. \tag{6}$$

Given that it is a triple vector product, we can manipulate (6) by permuting elements and arrive to

$$f^i_{EOP} = -[\boldsymbol{e}^i \times \hat{\boldsymbol{x}}^i_{SV}]^T \cdot \delta\boldsymbol{\theta}. \quad (7)$$

Replacing the LOS vector by its definition [11] leads us to a final expression of the EOP pseudorange fault vector as a function of the user position, the estimated satellite position and the EOP rotation vector,

$$f^i_{EOP} = \frac{1}{||\hat{\boldsymbol{x}}^i_{SV} - \hat{\boldsymbol{x}}_u||} \left([\hat{\boldsymbol{x}}_u\times] \cdot \hat{\boldsymbol{x}}^i_{SV}\right)^T \cdot \delta\boldsymbol{\theta} \quad (8)$$

where

$\hat{\boldsymbol{x}}^i_{SV}$	satellite position estimate vector
$\hat{\boldsymbol{x}}_u$	user position estimate vector.

Equation (8) explicitly separates the two inputs of the pseudorange error: first term is geometry-dependent and it's a function of the user ($\hat{\boldsymbol{x}}_u$) and satellites ($\hat{\boldsymbol{x}}^i_{SV}$) positions; second term ($\delta\boldsymbol{\theta}$) refers to the physical EOP mis-rotation carried out by the MCS/GCC. This will turn quite convenient in section IV when inspecting the fault vector (mode, magnitude and direction) and its role in the Residual Based RAIM approach.

Expanding to a subset of faulty satellites will entail some discussion about the constellation fault hypothesis. This consideration is not necessary for the ongoing derivation and it will be addressed in Section V. Without loss of generality, let us extend the derivation to a dual constellation scenario where Constellation A (n_A satellites in view) is affected by a common EOP event and Constellation B (n_B satellites in view) is fault free. The pseudorange error vector due to an EOP fault is expressed as follows:

$$\boldsymbol{f}_{EOP} = \begin{bmatrix} f^1_{EOP,A} \\ \vdots \\ f^{n_A}_{EOP,A} \\ f^1_{EOP,B} \\ \vdots \\ f^{n_B}_{EOP,B} \end{bmatrix}. \quad (9)$$

Since the EOP rotation vector is common to all of the satellites, the division between user-satellites geometry and EOP rotation contribution in (8) can be extrapolated to a matrix form. Matrix $\boldsymbol{T}$ (fault constraint matrix) collects in each row the projection vector of the corresponding pseudorange equation. The analysis of the fundamental subspaces of $\boldsymbol{T}$ will reveal the implications of the constrained constellation fault. Note that in the example fault vector in (10), measurements coming from Constellation B are EOP fault-free and hence the corresponding elements are zero,

$$\boldsymbol{f}_{EOP} = \begin{bmatrix} \frac{1}{r_1}\left([\hat{\boldsymbol{x}}_u\times] \cdot \hat{\boldsymbol{x}}^1_{SV,A}\right)^T \\ \vdots \\ \frac{1}{r_{n_A}}\left([\hat{\boldsymbol{x}}_u\times] \cdot \hat{\boldsymbol{x}}^{n_A}_{SV,A}\right)^T \\ 0 \\ \vdots \\ 0 \end{bmatrix} \cdot \begin{bmatrix} \delta\theta_x \\ \delta\theta_y \\ \delta\theta_z \end{bmatrix} = \boldsymbol{T} \cdot \delta\boldsymbol{\theta} \quad (10)$$

where

$\boldsymbol{f}_{EOP}$	pseudorange fault vector
r_i	user-satellite estimated range $\|\|\hat{\boldsymbol{x}}^i_{SV} - \hat{\boldsymbol{x}}_u\|\|$
$\hat{\boldsymbol{x}}^i_{SV,A}$	satellites position estimate vector
$\boldsymbol{T}$	fault constraint matrix.

The analysis of row vectors will reveal that matrix $\boldsymbol{T}$ is rank deficient. Equation (10) shows that all satellite position estimate vectors $\hat{\boldsymbol{x}}^i_{SV,A}$ are multiplied by the same infinitesimal rotation matrix $[\hat{\boldsymbol{x}}_u\times]$. For a given location, satellite position vectors undergo identical rotations and hence the resulting transformed vectors are all contained in the same subspace; column space of $[\hat{\boldsymbol{x}}_u\times]$. Annex A shows that this skew-symmetric matrix is rank deficient and its corresponding null space is formed by the set of vectors parallel to the rotation vector itself,

$$ker([\hat{\boldsymbol{x}}_u\times]) \equiv gen\{\hat{\boldsymbol{x}}_u\} \rightarrow dim(ker([\hat{\boldsymbol{x}}_u\times])) = 1 \quad (11)$$

Where $gen\{\hat{\boldsymbol{x}}_u\}$ is one-dimension subspace in $\mathcal{R}^3$ generated by vector $\hat{\boldsymbol{x}}_u$. According to the *rank-nullity theorem* [12], the dimension of the column space of $[\hat{\boldsymbol{x}}_u\times]$ is two implying that all the row vectors of $\boldsymbol{T}$ are contained in the same plane in $\mathcal{R}^3$. Applying basic algebraic properties we can show that

$$col([\hat{\boldsymbol{x}}_u\times]) = row(\boldsymbol{T}) = col(\boldsymbol{T}^T) \quad (12)$$

$$dim(col([\hat{\boldsymbol{x}}_u\times])) = dim(col(\boldsymbol{T}^T)) = 2 \quad (13)$$

$$dim(col(\boldsymbol{T}^T)) = dim(col(\boldsymbol{T})) = rank(\boldsymbol{T}) = 2. \quad (14)$$

Equation (10) presents $\boldsymbol{T}$ as the projection matrix that plots the EOP rotation fault vector $\delta\boldsymbol{\theta}$ into the pseudorange domain ($\boldsymbol{T} : \mathcal{R}^3 \rightarrow \mathcal{R}^n$). Given that $rank(\boldsymbol{T})$ is two, the column space of T is a subspace ($\mathcal{V}$) of dimension two in $\mathcal{R}^n$. Consequently, vector $\boldsymbol{f}_{EOP} \in \mathcal{V}$.

Here reside the particular properties of the EOP faults. Contrary to EOP, unconstrained constellation faults do not impose any condition over the elements of the pseudorange fault vector $\boldsymbol{f}$ which, in general, lies in a n_A-dimensional subspace. We will show in Section VI that reducing the dimension of the subspace where the fault vector is contained in will favorably impact the availability performance of the monitor against constellation faults.

It is worth to comment one last geometric aspect; the physical meaning of the null and row spaces of $\boldsymbol{T}$. Since the

row space of a matrix is orthogonal to its null space, according to (12) we can deduce that matrices $\boldsymbol{T}$ and $[\hat{\boldsymbol{x}}_u\times]$ have identical null spaces. In other words, EOP fault has null impact on the pseudorange error vector ($\boldsymbol{f}_{EOP} = 0$) when the EOP rotation axis coincides with the user position ($\delta\boldsymbol{\theta} \parallel \hat{\boldsymbol{x}}_u$) as stated in

$$ker(\boldsymbol{T}) = ker([\hat{\boldsymbol{x}}_u\times]) \rightarrow ker(\boldsymbol{T}) \equiv gen\left\{\hat{\boldsymbol{x}}_u\right\}. \quad (15)$$

Consequently, $row(\boldsymbol{T})$ should be a plane which is orthogonal to the user position vector in ECEF: local horizontal plane at the user location $\mathcal{H}$. This conclusion can be understood as follows: EOP faults only generate errors in the horizontal plane. However, since users may estimate their position solution by using both faulty and fault-free subsets (10), EOP fault will impact the position error in its vertical and horizontal components.

This last statement is a direct link to the previous EOP fault approach in user position domain [1]. The EOP constraint adds a horizontal nuisance parameter that only affects the subset of faulty satellites. Finally, the EOP constellation fault can be treated either as a fault vector that lies in a 2D space in the pseudorange domain or as fault that includes two additional horizontal parameters in the position domain.

III. INTEGRITY RISK EVALUATION FOR DUAL CONSTELLATION GNSS

In this section we formulate the risk evaluation method for detection only. Then, we characterize a model of the measurements for dual constellation GNSS. Finally we describe the least square estimator which, along with RAIM detector (Section IV) are used to evaluate the integrity risk.

A. Integrity Risk definition for detection only

The integrity risk or probability of hazardous misleading information (P_{HMI}) is defined as the join probability of the estimate error ε being larger than a specified alert limit l while the test statistic q remains lower than a detection threshold T,

$$P_{MHI} \equiv P(\mid \varepsilon \mid > l, \mid q \mid < T). \quad (16)$$

Let h be the number of fault hypotheses. P_{HMI} can be expressed considering a set of $h+1$ complementary, mutually exclusive hypotheses H_i (including the fault-free hypothesis H_0). Using the law of total probability, the criterion for availability of integrity [13] can be expressed as:

$$\begin{aligned} P_{HMI} &= \sum_{i=0}^{h} P(\mid \varepsilon \mid > l, \mid q \mid < T \mid H_i) P_{H_i} \\ &\leq I_{REQ} - P_{NM} \end{aligned} \quad (17)$$

where

ε	estimate error for the state of interest (least squares estimator)
l	alert limit specified by LPV-200 requirements [4]
q	Residual Based RAIM detection test statistic (Section IV)
T	detection threshold
H_i	set of hypothesis for $i = 0, .., .h$. Section V will cover the multi-satellite fault scenario and the different fault hypotheses.
P_{H_i}	Prior probability of fault occurence.
P_{NM}	Prior probability of the unmonitored events ($P_{NM} \ll I_{REQ}$)
I_{REQ}	Integrity Risk requirement specified in [4].

Equation (17) accounts for the contribution of each fault hypothesis to the total Integrity Risk (I_{risk}). Previous work has been done on the determination of the faults that need to be monitored and the associated probabilities of fault [14]. In this paper, we dive into the constellation fault hypotheses analyzing the feasibility of encountering faulty and fault-free subsets within the same constellation (Section V).

The continuity risk requirement $C_{REQ,0}$ sets a limit on the probability of false alarms. As a result, it is fulfilled by setting the value of the detection threshold as follows:

$$P(\mid q \mid \geq T) \mid H_0) P_{H_0} \leq C_{REQ,0}. \quad (18)$$

B. Measurement equation for dual constellation

In order to evaluate the integrity risk, the estimate error ε and the test statistic q need to be calculated using a measurement model [13]. In the case of multi-satellite or constellation faults, partitioning the measurement equation is convenient since it allows us to explicitly separate the faulty and fault-free subsets as we did in (9). For an example of dual constellation case, let n_A and n_B be the arbitrary number of available measurements from two different constellations and m the number of states respectively. The $(n_A + n_B) \times 1$ measurement vector $\boldsymbol{z}$ is modeled as:

$$\boldsymbol{z} = \boldsymbol{H}\boldsymbol{x} + \boldsymbol{\nu} + \boldsymbol{f}\ . \quad (19)$$

Measurement equations can be separated in two parts corresponding to each constellation as follows:

$$\begin{bmatrix} \boldsymbol{z}_A \\ \boldsymbol{z}_B \end{bmatrix} = \begin{bmatrix} \boldsymbol{H}_A \\ \boldsymbol{H}_B \end{bmatrix} \boldsymbol{x} + \begin{bmatrix} \boldsymbol{\nu}_A \\ \boldsymbol{\nu}_B \end{bmatrix} + \begin{bmatrix} \boldsymbol{f}_A \\ \boldsymbol{f}_B \end{bmatrix} \quad (20)$$

where

$\boldsymbol{H}_{A,B}$	observation matrix $n_A \times m$ and $n_B \times m$
$\boldsymbol{x}$	$m \times 1$ state vector
$\boldsymbol{\nu}_{A,B}$	measurements $n_A \times 1$ and $n_B \times 1$ noise vector
$\boldsymbol{f}_{A,B}$	fault vector $n_A \times 1$ and $n_B \times 1$.

Vectors $\boldsymbol{\nu}_{A,B}$ are assumed to be normally distributed with zero mean and covariance matrices $\boldsymbol{V_A}$ and $\boldsymbol{V_B}$ as follows:

$$\boldsymbol{\nu_A} \sim \boldsymbol{N(0, V_A)} \text{ and } \boldsymbol{\nu_B} \sim \boldsymbol{N(0, V_B)} \; . \tag{21}$$

The nominal measurement error model in this paper assumes that elements of the noise vector ν are independent. As a consequence, the matrices $\boldsymbol{V}_A$ and $\boldsymbol{V}_B$ are diagonal and the total covariance matrix can be expressed as a diagonal positive-definite matrix

$$\boldsymbol{V} = \begin{bmatrix} \boldsymbol{V}_A & \boldsymbol{0} \\ \boldsymbol{0} & \boldsymbol{V}_B \end{bmatrix}. \tag{22}$$

The nominal pseudorange error models are described in Section VI.

C. Least Squares Estimator

Weighted least-squares estimator is used to compute the position solution and its corresponding error. A detailed derivation of the estimator can be found in [11]. The state estimate vector $\hat{\boldsymbol{x}}$ and least-squares estimation matrix $\boldsymbol{S}$ are defined as

$$\hat{\boldsymbol{x}} = \boldsymbol{S}\boldsymbol{z} \text{ and } \boldsymbol{S} = (\boldsymbol{H}^T\boldsymbol{W}\boldsymbol{H})^{-1}\boldsymbol{H}^T\boldsymbol{W} \tag{23}$$

where the weighting matrix $\boldsymbol{W}$ is the inverse of the covariance matrix $\boldsymbol{V}$. The estimate error vector $\boldsymbol{\varepsilon}$ and its associated covariance matrix $\boldsymbol{P}$ are defined as:

$$\boldsymbol{\varepsilon} \equiv \hat{\boldsymbol{x}} - \boldsymbol{x} = \boldsymbol{S}(\boldsymbol{\nu} + \boldsymbol{f}) \tag{24}$$

$$\boldsymbol{\varepsilon} \sim N(\boldsymbol{S}\boldsymbol{f}, \boldsymbol{P}) \tag{25}$$

$$\boldsymbol{P} = (\boldsymbol{H}^T\boldsymbol{W}\boldsymbol{H})^{-1}. \tag{26}$$

In order to be consistent with the nomenclature followed in the previous Section II, note that the state estimate vector $\hat{\boldsymbol{x}}$ contains, together with the two clock biases (b_A and b_B for GPS and for Galileo, respectively), the estimated user position $\hat{\boldsymbol{x}}_u$ utilized in the EOP fault description in (10).

Finally, the estimate error of the single state of interest can be obtained by extracting the corresponding row $\boldsymbol{s}^T$ of the least-squares estimation matrix $\boldsymbol{S}$. Let us particularize for the vertical coordinate (although it can be applied to the horizontal coordinates):

$$\boldsymbol{s}^T = \boldsymbol{\alpha}^T\boldsymbol{S} \text{ and } \boldsymbol{\alpha}^T = [0\ 0\ 1\ 0\ 0] \, . \tag{27}$$

The vertical estimation error variance σ_V^2 is simply obtained by selecting the corresponding diagonal element of the error covariance matrix. As result, the state of interest, vertical in this example, is obtained as follows:

$$\varepsilon = \boldsymbol{\alpha}^T\boldsymbol{\varepsilon} = \boldsymbol{s}^T(\boldsymbol{\nu} + \boldsymbol{f}) \tag{28}$$

$$\varepsilon \sim N(\boldsymbol{s}^T\boldsymbol{f}, \sigma_V^2) \tag{29}$$

$$\sigma_V^2 = \boldsymbol{\alpha}^T\boldsymbol{P}\boldsymbol{\alpha} \; . \tag{30}$$

IV. RESIDUAL BASED RAIM AGAINST CONSTELLATION FAULTS

This sections describes and analyzes the test statistic which is the second term required to evaluate the Integrity Risk expressed in (17). Traditionally, there are two different approaches to asses the test statistic: position domain and measurement (or pseudorange) domain. As seen in Section II, the EOP fault can be constrained by performing a rotation of the measurements in the pseudorange domain. This paper utilizes the Residual Based RAIM approach to evaluate the impact of a constrained constellation fault on the test statistic and ultimately on the integrity risk.

A. Residual Based RAIM

The detection test statistic q is derived from the pseudorange residual vector [15]. The residual vector is defined as:

$$\boldsymbol{r} \equiv \boldsymbol{z} - \boldsymbol{H}\hat{\boldsymbol{x}} = (\boldsymbol{I} - \boldsymbol{H}\boldsymbol{S})\boldsymbol{z} = (\boldsymbol{I} - \boldsymbol{H}\boldsymbol{S})(\boldsymbol{\nu} + \boldsymbol{f}) \tag{31}$$

where $\boldsymbol{I}$ is the $(n \times n)$ identity matrix. Residual Based RAIM approach is based on the use of the magnitude of the residual vector as a test statistic. The residual-based test statistic q^2 is the weighted norm of $\boldsymbol{r}$ [13]

$$q^2 = \boldsymbol{r}^T\boldsymbol{W}\boldsymbol{r} \; . \tag{32}$$

Under a fault hypothesis, test statistic follows a non-central χ^2 distribution with $(n - m)$ degrees of freedom and non centrality parameter λ:

$$q^2 \sim \chi^2(n - m, \lambda^2) \tag{33}$$

$$\lambda^2 = \boldsymbol{f}^T\boldsymbol{W}(\boldsymbol{I} - \boldsymbol{H}\boldsymbol{S})\boldsymbol{f} \; . \tag{34}$$

Under nominal conditions ($\boldsymbol{f} = 0$), test statistic follows a central χ^2 distribution ($\lambda = 0$) with $(n - m)$ degrees of freedom .

$$q_{FF}^2 \sim \chi^2(n - m) \tag{35}$$

B. EOP Constellation Fault vector in Residual Based RAIM

The fault vector can be interpreted as a measurement bias due to a rare event which is not covered by the nominal error model. It is characterized by its *fault mode* which defines the subset of faulty satellites in view; its *fault magnitude* which is the Euclidean norm of the fault vector; and

its *fault direction* which establishes a relative relationship between the vector's elements [13]. In general, considering the fault magnitude and direction is cumbersome since they are unknown. The approach that we will follow in this paper is to overbound each fault hypothesis with the worst case fault vector $\bar{\boldsymbol{f}}_i$. This vector maximizes the Integrity Risk for a given fault hypothesis [16] and it can be expressed as

$$P(|\,\varepsilon\,|>l, |\,q\,|<T|H_i) \leq P(|\,\varepsilon\,|>l, |\,q\,|<T|\bar{\boldsymbol{f}}_i) \quad (36)$$

It is proved in [13] that both distribution ε and q are statistically independent, and therefore the join probability in (36) can be reformulated as follows:

$$\begin{aligned} &P(|\,\varepsilon\,|>l, |\,q\,|<T|\bar{\boldsymbol{f}}_i) = \\ &P(|\,\varepsilon\,|>l|\bar{\boldsymbol{f}}_i)\; P(q\,|<T|\bar{\boldsymbol{f}}_i)\;. \end{aligned} \quad (37)$$

As in [13], let us define the square of the failure mode slope as the ratio of the squared mean of the estimate error over the squared non-centrality parameter of the test statistic:

$$g^2_{F_i} \equiv \frac{\boldsymbol{f}_i^T \boldsymbol{s}\boldsymbol{s}^T \boldsymbol{f}_i}{\boldsymbol{f}_i^T \boldsymbol{W}(\boldsymbol{I}-\boldsymbol{H}\boldsymbol{S})\boldsymbol{f}_i}\;. \quad (38)$$

The failure mode slope depends on the fault mode and direction but not on the fault magnitude [17]. In the case of Constrained Constellation Fault (CCF), we can benefit from (10) where geometric and EOP rotation contribution are explicitly separated. Following the derivation in [13] and we can particularize the failure mode slope as follows:

$$g^2_{CCF} = \frac{\delta\boldsymbol{\theta}^T \boldsymbol{A}^T \boldsymbol{B}^T \boldsymbol{B}\boldsymbol{A}\delta\boldsymbol{\theta}^{\boldsymbol{T}}}{\delta\boldsymbol{\theta}^T \delta\boldsymbol{\theta}} \quad (39)$$

where

$$\boldsymbol{A} = \left[\boldsymbol{T}^T \boldsymbol{W}(\boldsymbol{I}-\boldsymbol{H}\boldsymbol{S})\boldsymbol{T}\right]^{-1/2}$$

$$\boldsymbol{B} = \boldsymbol{s}^T \boldsymbol{T}\;.$$

The worst case fault vector, which overbounds the Integrity Risk, maximizes the failure mode slope. Under a multi-measurement fault hypothesis (a given fault mode) the worst-case failure mode slope $\bar{g}_{CCF}$ can be expressed as a function of the geometry as

$$\bar{g}^2_{CCF} = \boldsymbol{s}^T \boldsymbol{T}\left[\boldsymbol{T}^T \boldsymbol{W}(\boldsymbol{I}-\boldsymbol{H}\boldsymbol{S})\boldsymbol{T}\right]^{-1}\left(\boldsymbol{s}^T \boldsymbol{T}\right)^T \quad (40)$$

As mentioned, the failure mode slope establishes a link between the mean of the estimate error μ_ε and the non-centrality parameter λ. In other words, in a failure mode plot of ε versus q, μ_ε and λ caused by a fault of magnitude ranging from $-\infty$ to $+\infty$ describe a line of slope $\bar{g}_{CCF}$ passing through the origin. Let us analyze the role of matrix $\boldsymbol{T}$ in the worst-case failure mode slope.

EOP constraint manifests itself through matrix $\boldsymbol{T}$. As shown in Section II, EOP fault vector is contained in a subspace of dimension two in the pseudorange domain ($\boldsymbol{f}_{EOP} \in \mathcal{V}$). As a consequence, under a constellation fault hypothesis, the constrained worst-case fault vector direction is forced to lie in that subspace consequently limiting the worst-case slope value. For the unconstrained case, that subspace will have dimension n_A since $\boldsymbol{T}$ is a diagonal $n \times n$ matrix with one and zero elements in the corresponding faulty and fault-free positions.

Figure 1 is a conceptual representation of the effect of the common rotation constraint under a constellation fault hypothesis. The abscissa represents the test statistic distribution q while the ordinate represents the vertical estimate error ε distribution. According to P_{HMI} definition in (16), Hazardous Misleading Information (HMI) area corresponds to the region where the error ε is larger than the alert limit l and the detection test statistic q is below the threshold T. The common rotation embedded in matrix $\boldsymbol{T}$ substantially reduces the value of the worst-case slope from the unconstrained constellation fault $\bar{g}_{UCF}$ to the constrained case $\bar{g}_{CCF}$. This reduction in the slope directly impacts the mean of the estimate error μ_ε making the fault less hazardous for a given fault magnitude. As a result, it implies a distancing from the HMI area which means a decrease of the Integrity Risk. According to the criterion for availability of integrity in (17) this consequently entails an improved availability performance.

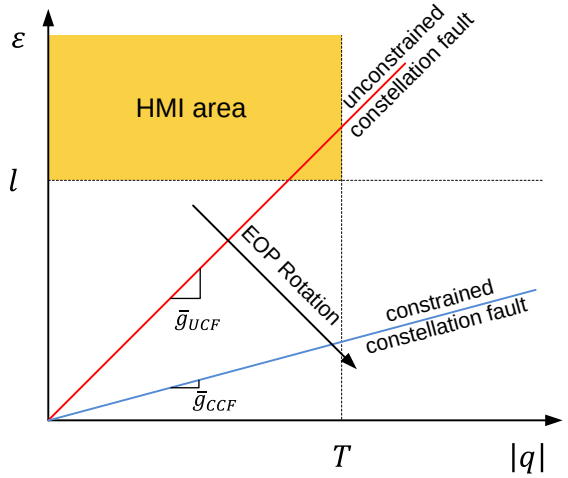

Figure 1: Failure mode worst-case slopes comparison

In this section we anticipate some results by quantitatively demonstrating the effect of the constraint in the slope (error model and constellation details in Section VI). Table 1 compares the worst-case mode slope values for the unconstrained and constrained cases. For an example location

under a GPS-Galileo dual constellation scenario, first column represents the worst-case slope of an unconstrained GPS constellation-wide fault mode while second column shows the worst-case slope for the same GPS constellation fault constrained by an EOP coherent rotation (matrix $\boldsymbol{T}$). Third and fourth columns indicate the number of GPS and Galileo satellites in view for each of the four displayed geometries.

Table 1: Worst-case failure mode slope reduction

$\bar{g}_{UCF}$	$\bar{g}_{CCF}$	n_{GPS}	n_{Gal}
1.8226	0.2243	9	8
1.9060	0.2226	7	7
1.6532	0.4219	8	6
2.2011	0.1476	8	6

C. EOP monitor Minimum Detectable Error

We can also quantify the effect of the EOP constraint by computing the Minimum Detectable Error (MDE). It is a typical way to evaluate the performance of a monitor but for comparison purposes it helps to visualize the relative performance of the constrained case versus the unconstrained one. Table 2 uses identical geometries and fault hypothesis as table 1 to compare the decrease of the MDE when imposing the constraint. First column accounts for the unconstrained case while second column accounts for the constrained one.

Table 2: Minimum detectable error reduction

MDE Unconstr. CF (m)	MDE Constr. CF (m)
17.11	2.11
17.34	2.03
15.04	3.84
20.03	1.34

Results in Table 2 can be interpreted as follows: for a given detection threshold T that fulfills the continuity requirement in (18), the misdetection probability substantially decreasing causing a total reduction of the integrity risk. We can conclude the section stating that the satellites common rotation provided by (10) decreases the Integrity Risk by two effects: first, it makes the fault less hazardous; second, it makes the fault more detectable.

V. EOP CONSTELLATION FAULT SCENARIO

The derivation outlined throughout previous sections can be applied to different EOP constellation fault hypothesis just by adapting the faulty subset of satellites. This paper classifies the constellation fault scenario attending to the dependency of the EOP fault across constellation which refers to the join probability of occurrence of the dual constellation fault. GPS Master Control Station and Galileo Control Center obtain the EOP Predictions from different international sources. Further investigation on the correlation of Galileo and GPS EOPP is left for future work. In this paper we separately analyze two scenarios concerning the constellations independence for GPS-Galileo dual constellation users:

- EOP Single Constellation (SC) Fault
- EOP Cross Constellation (CC) Fault

First scenario assumes that GPS and Galileo EOPP undergo separate estimation process and therefore the cross constellation is a join event of two independent faults. Second one considers that the same source of the EOPP GPS fault can originate a concurrent fault in Galileo, and hence the cross constellation faults are not independent.

Regarding the single satellite faults, [14] describes an algorithm for the determination of the faults that need to be monitored and the corresponding unmonitored P_{NM} that should be accounted as seen in (17). The two different scenarios will be numerically implemented in Section VI.

As shown in (36), we overbound the P_{HMI} by choosing the worst case fault. In order to avoid hypothesizing about fault magnitude, given a fault mode and direction which define the failure mode slope , we look for the fault magnitude that maximizes the Integrity Risk using a line-search method.

A. EOP Single Constellation (SC) Fault

This scenario assumes that GPS and Galielo EOP faults are independent and have a similar prior probability of occurrence P_{const}. The hypothesis of simultaneous independent Single Constellation faults cannot be taken into account since ARAIM monitor will be ineffective (residual vector is zero) [7]. As a result, the probability of this join event P^2_{const} should be included in the non monitored P_{NM}. The set of single constellation faults hypothesis consists of:

$$H^{SC}_{EOP} = \left\{ \begin{bmatrix} f^{gps}_1 \\ \vdots \\ f^{gps}_{n_{gps}} \\ 0 \\ \vdots \\ 0 \end{bmatrix}, \begin{bmatrix} 0 \\ \vdots \\ 0 \\ f^{gal}_1 \\ \vdots \\ f^{gal}_{n_{gal}} \end{bmatrix} \right\} \tag{41}$$

where

$$P^{SC}_{EOP} = P_{const} \ .$$

B. EOP Cross Constellation Fault (ICC)

This scenario expands the previous SC by assuming that GPS and Galileo EOP faults have a common source and hence they can occur simultaneously with the same probability P_{const}. As a result, EOP subsets of faulted satellites

across constellations should be considered. As it can be foreseen, the size of this subset will have a tremendous impact in the availability performance. The scope of this fault scenario is to determine the maximum affordable number k of simultaneously faulted satellites beyond which ARAIM availability drops. CC set of hypothesis H_{EOP}^{CC} is defined the set of $(2^k - 1)$ cross constellation subsets that includes up to k GPS and/or Galileo faulty satellites:

$$H_{EOP}^{CC} = \left\{ \underbrace{\begin{bmatrix} f_1^{gps} \\ \vdots \\ 0 \\ f_1^{gal} \\ \vdots \\ 0 \end{bmatrix} \cdots \begin{bmatrix} f_1^{gps} \\ \vdots \\ f_{n_{gps}}^{gps} \\ f_1^{gal} \\ \vdots \\ 0 \end{bmatrix} \cdots \begin{bmatrix} f_1^{gps} \\ \vdots \\ f_{n_{gps}}^{gps} \\ 0 \\ \vdots \\ f_{n_{gal}}^{gal} \end{bmatrix} \cdots}_{(2^k-1)\ Cross\ Constellation\ Faults} \right\} \quad (42)$$

$$P_{EOP}^{CC} = P_{const} \ .$$

VI. AIRCRAFT LPV-200 PRECISION APPROACH

This section presents a performance evaluation of the described ARAIM monitor against EOP faults. As already mentioned, we quantify availability performance of the EOP monitor under the two described fault scenarios from Section V. Table 3 summarizes the simulation parameters including ARAIM single-measurements faults, constellation faults and error models. It also includes LPV-200 navigation requirements to support localizer precision vertical approach operations down to 200 feet above the ground. More detailed description can be found in [1].

Table 3: Simulation Parameters

SV clock and orbit error (URA)	$0.75\ m$ for GPS $0.957\ m$ for Galileo
Residual tropospheric error	$0.12\frac{1.001}{(0.002001+sin^2\xi)^{1/2}}\ m$
Smoothed code multipath	$0.13 + 0.53e^{-\xi/10}\ m$ for GPS (lookup table for Galileo [1])
Smoothed code receiver noise	$0.15 + 0.43e^{-\xi/6.9}\ m$
Fault-free meas. bias b_{MAX}	$0.75\ m$ for GPS $1\ m$ for Galileo
Integrity risk requirement	10^{-7}
Continuity risk requirement	$2 \cdot 10^{-6}$
Prior probability of satellite fault P_{sat}	10^{-5}
Prior probability of const. fault P_{const}	10^{-4}

ξ is the satellite elevation angle in degrees

Simulations work with a '24-1' GPS constellation and a '27-1' Galileo constellation, which are the nominal constellations with one spacecraft removed to account for outages. Given that the navigation requirements are normally more difficult to fulfill for the vertical coordinate, the following results will only focus on this coordinate. Under LPV-200 requirements, the target Vertical Alert Limit (VAL) is $l = 35\ m$. Availability results will be showed for a 10×10 deg grid of locations and simulation time of 24 hours. Availability is computed at each location as a fraction of time where P_{HMI} meets the integrity risk requirement I_{REQ}. Regarding coverage, it is defined as the percentage of grid point locations exceeding a certain availability; coverage and average availability computations are weighted at each location by the cosine of the location's latitude, because grid point locations near the equator represent larger areas than near the poles [16].

A. EOP Single Constellation (SC) Fault

Figure 2 represents the availability map for an alert limit of 35 m under unconstrained SC fault hypothesis. Second row of table 4 shows that, for the unconstrained case, the coverage of 99.9% availability is 38.35% and the average availability is 99.01%. When imposing the EOP constraint, the results substantially enhance obtaining a 99.9% coverage of 100% (third row of table 4), which implies a uniform color in the availability map shown in figure 3.

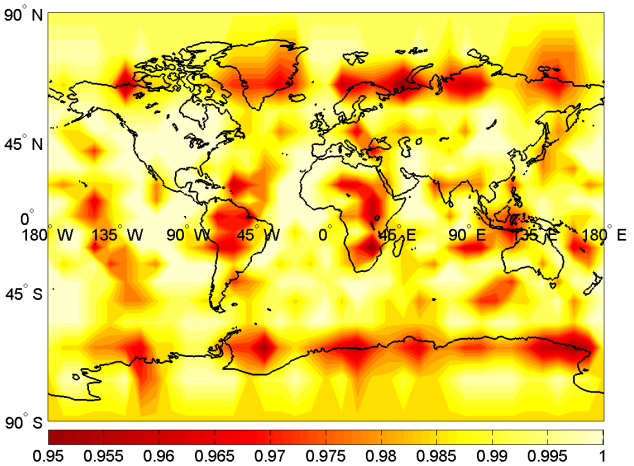

Figure 2: Availability map for unconstrained single constellation fault, VAL=35 m

Table 4: Coverage table for single constellation fault, VAL=35m

Constel. Fault	Cov.99.9%	Av.Avail.
Unconstrained	38.35%	99.01%
Constrained	100%	100%

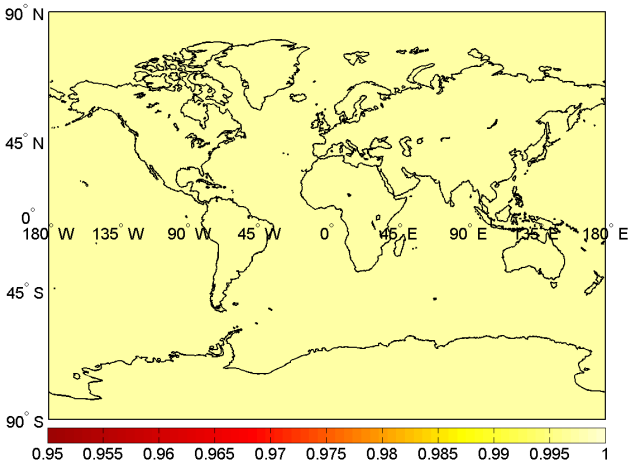

Figure 3: Availability map for constrained single constellation fault, VAL=35 m

In order to analyze the ceiling of the performance of EOP constraint under Single Constellation faults, let us reduce the alert limit to 20 m and reevaluate the coverage values. Table 5 shows that even reducing the alert limit, EOP constrained largely enhance the coverage results as it can be seen in its second column. In addition figure 4 represents the availability map for an alert limit of 20 m under constrained SC fault hypothesis.

Table 5: Coverage table for single constellation fault, VAL=20m

Constel. Fault	Cov. 99.9%	Av.Avail.
Unconstrained	0	62.57
Constrained	93.59	99.93

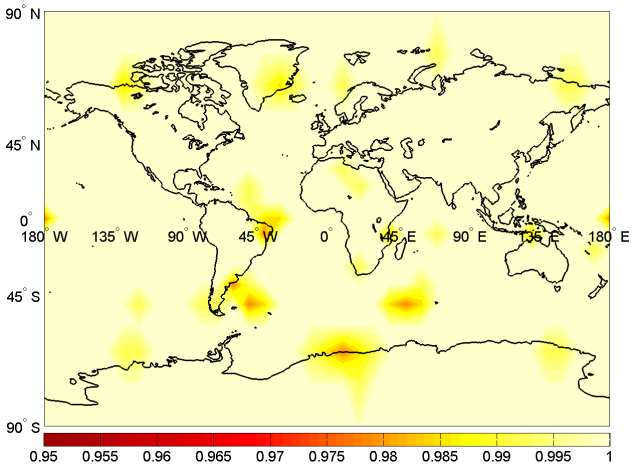

Figure 4: Availability map for constrained single constellation fault, VAL=20 m

B. EOP Cross Constellation (CC) Fault

As expected, this scenario is more pessimistic. The fact that both constellations can be simultaneous affected by an EOP fault causes the performance to drop. The aim of this study is to determine the maximum affordable size of the cross constellation hypothesis subset. In this section, we will not compare the relative performance between constrained and unconstrained hypothesis since the first ones are already quite affected. Table 6 gathers the coverage results a for worst-case subset (the one that maximizes the integrity risk) formed by 2, 3 and 4 satellites respectively. As it can be seen, just for a subset of 2 satellites (which is the minimum size we can have to declare a cross constellation fault) the coverage of 99.9% is 93.93%. In addition, figure 5 shows the availability map for a maximum size of cross constellation subset of two.

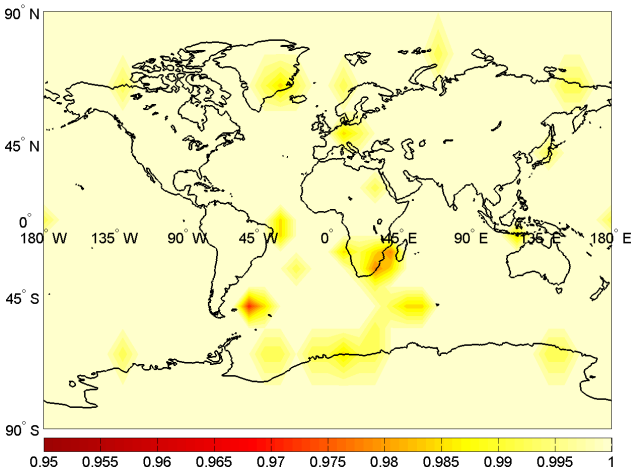

Figure 5: Availability map constrained cross constellation fault , maximum size of subsets 2 and VAL=35 m

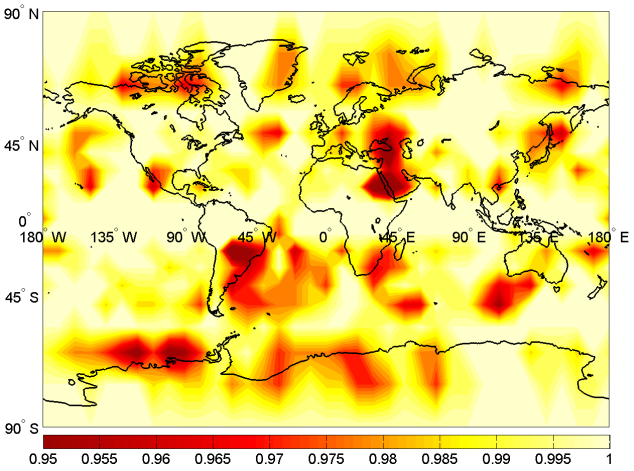

Figure 6: Availability map constrained cross constellation fault , maximum size of subsets 3 and VAL=35 m

Table 6: Coverage table for constrained cross constellation fault, VAL=35 m

Subset size	Cov. 99.9%	Av.Avail.
2	93.93%	99.93%
3	55.12%	99.21%
4	23.26%	97.36%

VII. CONCLUSION

This paper has developed a new Residual Based RAIM fault monitor in the context of LPV-200 precision approach against EOP faults. Through an analytical derivation, this work demonstrates that the EOP fault is constrained and the corresponding pseudorange error vector lies in a 2D subspace. This subspace is the projection of the local horizontal plane at the user location into the pseudorange domain. Under an EOP event, this constraint reduces both the mean of the estimate position error distribution and the probability of misdetection which ultimately decreases the Integrity Risk. As a result, ARAIM can protect against EOP constellation faults if we consider them independent across constellations.

Finally, this paper has shown that dual constellation ARAIM cannot afford common dependent EOP cross-constellation faults even for subsets larger than two satellites. One solution for mitigation is the control of the inter-constellation updating process. Cross constellation fault scenario can be suppressed by avoiding simultaneous constellations updates. In that case, we can overlook the cross constellation faulty subsets which severely weaken the geometry. Other solution can be implemented at the user level via comparison of current broadcast ephemerides with previously validated broadcast ephemerides (which does not rely on the independence across constellations). In any case, the across constellations independence is still under study and future revisions of this work will dive into the GPS-Galileo EOPP correlation.

ANNEX A. NULL SPACE AND RANK OF THE SKEW-SYMMETRIC MATRIX

Here we demonstrate that skew-symmetric matrix $[\hat{\boldsymbol{x}}_u\times]$ is rank deficient and its corresponding null space is formed by the set of vectors parallel to the rotation vector $\hat{\boldsymbol{x}}_u$ itself. Formally, the null space (or *kernel*) of a $(n \times n)$ matrix $\boldsymbol{A}$ is defined as the set of vectors in $\mathcal{R}^n$ that fulfill:

$$Null(\boldsymbol{A}) = ker(\boldsymbol{A}) = \{\boldsymbol{v} \in \mathcal{R}^n : \boldsymbol{A}\boldsymbol{v} = \boldsymbol{0}\} \ .$$

Let us rename the skew-symmetric matrix $\boldsymbol{R} = [\hat{\boldsymbol{x}}_u\times]$ The null space of $\boldsymbol{R}$ can be found by solving the following system of equations:

$$\boldsymbol{R}\boldsymbol{v} = \boldsymbol{0} \ .$$

It can be reduced by simply applying Gaussian Elimination

$$\left[\begin{array}{ccc|c} 0 & -x_{u,3} & x_{u,2} & 0 \\ x_{u,3} & 0 & -x_{u,1} & 0 \\ -x_{u,2} & x_{u,1} & 0 & 0 \end{array}\right] \rightarrow$$

$$\left[\begin{array}{ccc|c} -x_{u,2} & x_{u,1} & 0 & 0 \\ 0 & x_{u,1}x_{u,3} & -x_{u,1}x_{u,2} & 0 \\ 0 & -x_{u,1}x_{u,3} & -x_{u,1}x_{u,2} & 0 \end{array}\right] \rightarrow$$

$$\left[\begin{array}{ccc|c} -x_{u,2} & x_{u,1} & 0 & 0 \\ 0 & x_{u,1} & -x_{u,2} & 0 \\ 0 & 0 & 0 & 0 \end{array}\right] \rightarrow$$

$$\boldsymbol{v} = \gamma \begin{bmatrix} x_{u,1} \\ x_{u,2} \\ x_{u,3} \end{bmatrix} \ ; \ \gamma \in \mathcal{R} \ .$$

The solution of the system of equations is the set of vectors which are parallel to $\hat{\boldsymbol{x}}_u$. As a result the null space of the skew-symmetric can be defined as:

$$ker([\hat{\boldsymbol{x}}_u\times]) = gen\{\hat{\boldsymbol{x}}_u\}$$

where $gen\{\hat{\boldsymbol{x}}_u\}$ is one-dimension subspace in $\mathcal{R}^3$ generated by vector $\hat{\boldsymbol{x}}_u$. According to the rank-nullity theorem [12], the rank of the skew-symmetric matrix is two (rank deficient).

REFERENCES

[1] "Interim report, issue 1.0," Working Group C, ARAIM Technical Subgroup, EU-US Cooperation in Satellite Navigation, December 19th, 2012.

[2] J. Blanch, T. Walter, P. Enge, S. Wallner, F. Amarillo, R. Dellago, R. Ioannides, I. Fernandez, B. Belabbas, A. Spletter, and M. Rippl, "Critical elements for a Multi-Constellation Advanced RAIM," *NAVIGATION, Journal of the Institute of Navigation*, vol. 60, no. 1, pp. 53–69, Spring 2013.

[3] "Global positioning system standard positioning service performance standard." U.S. Department of Defence, 4th Ed. September 2008, pp A-22.

[4] "Minimum Aviation System Performance Standards for the Local Area Augmentation System (LAAS)." RTCA Special Committee 159, RTCA/DO-245, 2004, Appendix D.

[5] Y. Bock, *Reference Systems*, ch. 1, pp. 1–41. Lecture notes in earth sciences, Berlin; Heidelberg; New York; Barcelona; Budapest; Hong Kong; London; Milan; Paris; Singapore; Tokyo: Springer, second edition ed., 1998 1998. n/a.

[6] "Chapter 5 of IERS Technical Note 36: Transformation between the International Terrestrial Reference System and the Geocentric Celestial Reference System." International Earth Rotation and Reference Systems Service, 2010.

[7] Y. C. Lee, "New Advanced RAIM with improved availability for detecting Constellation-Wide faults, using two independent constellations," *NAVIGATION, Journal of the Institute of Navigation*, vol. 60, no. 1, pp. 71–83, Spring 2013.

[8] C. Gruber, "GPS Program Update to Civil GPS Service Interface Committee (CGSIC)," 18 Sep 2012.

[9] Observatoire de Paris, Earth Orientation Center, http://hpiers.obspm.fr/eop-pc/.

[10] S. Langel, F.-C. Chan, J. Meno, M. Joerger, and B. Pervan, "Detecting Earth Orientation Parameter (EOP) Faults for High Integrity GNSS Aviation Applications," in *International Technical Meeting (ITM) of The Institute of Navigation, San Diego, CA*, January 28-30, 2013.

[11] P. Misra and P. Enge, *Global Positioning System, Signals, Measurements, and Performance*. Ganga-Jamuna Press, 2nd ed., 2006.

[12] C. D. Meyer, *Matrix Analysis and Applied Linear Algebra*. SIAM, 2000.

[13] M. Joerger, F.-C. Chan, S. Langel, and B. Pervan, "RAIM Detector and Estimator Design to Minimize the Integrity Risk," in *25th International Technical Meeting of the Satellite Division of The Intitute of Navigation, Nashville TN*, September 17-21, 2012.

[14] J. Blanch, T. Walter, P. Enge, Y. Lee, B. Pervan, M. Rippl, and A. Spletter, "Advanced RAIM User Algorithm Description: Integrity Support Message Processing, Fault Detection, Exclusion, and Protection Level Calculation," in *25th Internation Technical Meeting of the Satellite Division of The Institute of Navigation, Nashville, TN*, September 17-21, 2012.

[15] B. Pervan, *Navigation Integrity for Aircraft Precision Landing Using the Global Positioning System*. PhD thesis, Stanford University, March 1996.

[16] M. Joerger and B. Pervan, "Solution Separation and Chi-Squared ARAIM for Fault Detection and Exclusion," in *Proceedings of the 2014 IEEE/ION Position, Location and Navigation Symposium, Monterey, CA*, May 5-8, 2014.

[17] J. E. Magnus, "RAIM with Multiple Faults," *NAVIGATION, Journal of the Institute of Navigation*, vol. 53, no. 4, Winter 2006.